Biosensors and Bioelectronics 44 (2013) 171–176

Contents lists available at SciVerse ScienceDirect

Biosensors and Bioelectronics

journal homepage: www.elsevier.com/locate/bios

A label-free microRNA biosensor based on DNAzyme-catalyzed and microRNA-guided formation of a thin insulating polymer film

Wei Shen, Huimin Deng, Yuqian Ren, Zhiqiang Gao*

Department of Chemistry, National University of Singapore, Singapore 117543, Singapore

ARTICLE INFO

Article history:
Received 18 October 2012
Received in revised form
12 January 2013
Accepted 15 January 2013
Available online 23 January 2013

Keywords:
MicroRNA
DNAzyme
Nuclease I
3,3′-Dimethoxybenzidine
Electrochemical impedance

ABSTRACT

Herein we report a label-free microRNA (miRNA) biosensor in which the formation of a thin insulating film is used to amplify the analytical signal. Briefly, the biosensor is made of an oligonucleotide-coated gold electrode. After hybridizing with a target miRNA, free capture probe (CP) strands on the biosensor are removed by a nuclease digestion. A second hybridization with an oligonucleotide-tailed DNAzyme is performed to introduce the DNAzyme to the biosensor. The DNAzyme triggers the polymerization of 3,3′-dimethoxybenzidine (DB) in the presence of H_2O_2 and the hybridized miRNA-CP duplexes serve as templates to guide the deposition of poly (3,3′-dimethoxybenzidine) (PDB). The formation of the insulating PDB film alters the impedance of the biosensor, rendering it readily distinguishable by electrochemical impedance measurements. The accumulative nature of the PDB deposition drastically improves the detectability of the biosensor. A proof-of-concept study is conducted on the detection of miRNAs in total RNA extracted from cultured cells.

1. Introduction

MicroRNAs (miRNAs) are highly conserved small RNAs that regulate the expression of genes by binding to the 3′-untranslated regions of messenger RNAs (mRNAs) through a dual-mechanism: translational repression and target degradation (Bartel, 2004; Engels and Hutvagner, 2006). It is believed that over 50% of all protein encoding genes in humans are regulated by miRNAs. Increasing evidence has shown that, in addition to their regulatory roles in gene expression, miRNAs are linked to various physiological and pathological processes, and cancerous diseases in particular (Esquela-Kerscher and Slack, 2006; Stefani and Slack, 2008). It is also believed that miRNAs are directly associated with patients' individual responses to diseases, drugs, and other environmental factors. Therefore, miRNAs have great potential in therapeutics, drug discovery, and molecular diagnostics (Lu et al., 2005, Volinia et al., 2006). The development of diagnostic techniques to enable miRNA detection at point-of-care is of paramount importance for early disease diagnosis and prognosis.

Unlike DNA and mRNA, the unique attributes of miRNAs, such as their short lengths, inherently different melting temperatures, and high sequence similarities among members of an miRNA family, make miRNA detection with high sensitivity and specificity technically demanding (Pritchard et al., 2012). A number of approaches, such as microarrays (Thomson et al., 2004), quantitative real-time PCR (qRT-PCR) (Chen et al., 2005; Raymond, et al., 2005), and direct labeling and amplified detection (Liang et al., 2005; Gao and Yang, 2006; Gao and Yu, 2007; Peng and Gao, 2011), have been proposed. In spite of the existence of various miRNA detection techniques with acceptable detection sensitivity and specificity, they are yet to be adaptable for point-of-care use. The main obstacle lies in the requirements for special laboratory skills in miRNA tagging and for complex instruments in signal readout (Pritchard et al., 2012). Label-free and PCR-free electrochemical approaches that enable sensitive detection of miRNAs with portable instruments are highly desirable for the development of miRNA expression profiling platforms. In this regard, electrochemical impedance spectroscopy (EIS)-based detection is one of the promising candidates. Besides the attractive features of electronic detection like inherent miniaturization, good compatibility with advanced semiconductor technology, and low cost, EIS-based biosensors are largely nondestructive, do not require molecular labeling of a target analyte—label-free detection, capable of real-time detection, and highly sensitive to the presence of minute amounts of any electron-transfer impeding material on the biosensor surface. A major drawback is that EIS tests are much more time-consuming than their voltammetric and amperometric counterparts.

In this report, we proposed for the first time an EIS biosensor together with a polymer deposition-based amplification protocol that enables label-free detection of miRNAs with enhanced sensitivity. The biosensor was based on direct hybridization of target miRNAs and the use of DNAzyme. The DNAzyme effectively catalyzed the polymerization of 3,3′-dimethoxybenzidine (DB) and the hybridized miRNA-capture probe (CP) duplexes guided the deposition of poly (3,3′-dimethoxybenzidine) (PDB). Taking advantage of this monomer-replicating concept and the cumulative

* Corresponding author. Tel.: +65 6516 3887; fax: +65 6779 1691.
E-mail address: chmgaoz@nus.edu.sg (Z. Gao).

0956-5663/$ - see front matter © 2013 Elsevier B.V. All rights reserved.
http://dx.doi.org/10.1016/j.bios.2013.01.028

nature of the polymer formation process (Qian and He, 2009; Peng and Gao, 2011), a detection limit of 2.0 fM was accomplished. The demonstrated label-free detection of miRNAs marked an encouraging step toward the development of a portable miRNA expression profiling platform for uses at point-of-care.

2. Experimental section

2.1. Materials and apparatus

Hemin (> 98%), 4-mercaptoaniline (MAn, 97%), DL-Dithiothreitol (DTT, > 99%) were from Sigma-Aldrich (St Louis, MO). Synthetic miRNAs, thiolated oligonucleotide CPs, DNAzyme, and all other oligonucleotides of PCR purity were from Proligo (Singapore). DNA Exonuclease I was supplied by New England Biolabs (Ipswich, MA). Total RNA extraction and miRNA enrichment kits were from Qiagen (Singapore). All other reagents were purchased from Sigma-Aldrich and used without further purification. TE buffer (10 mM Tris–HCl + 1.0 mM EDTA + 0.10 M NaCl) was used as hybridization and washing buffer. PDB deposition cocktail used in this work contained 50 mM H_2O_2 and 1.0 mM DB in pH 7.0 0.10 M phosphate buffer.

Electrochemical experiments were conducted with an IM6 electrochemical workstation (Zahner Elektrik, Germany). A three-electrode system, consisting of the biosensor, a nonleak Ag/AgCl reference electrode (Cypress Systems, Lawrence, KS), and a platinum foil counter electrode, was used in all electrochemical measurements. EIS tests were performed in 0.10 M sodium sulfate containing 2.5 mM of $K_3Fe(CN)_6$ and 2.5 mM $K_4Fe(CN)_6$, over a frequency range from 100 KHz to 10 mHz with a 5-mV sinusoidal voltage perturbation and a bias potential of 0.17 V (vs. Ag/AgCl). $Fe(CN)_6^{3-}$/$Fe(CN)_6^{4-}$ in the 0.10 M sodium sulfate solution serve as redox probes so as to perform EIS. All potentials reported in this work were referred to the Ag/AgCl reference electrode. UV–vis experiments were conducted with a V-570 UV/VIS spectrophotometer (JASCO Corp., Japan).

2.2. Fabrication of the biosensor

Before CP immobilization, a gold electrode was thoroughly polished with 0.05 μm alumina slurry and cleaned in water and ethanol in an ultrasonic bath for 10 min, respectively. Immobilization of the thiolated CPs on the cleaned gold electrode was achieved following a published procedure with slight modification (Peng and Gao, 2011). Briefly, the thiolated CPs were treated with 0.10 M DTT in phosphate-buffered saline (PBS) for 60 min and then purified using a NAP-10 column. CP immobilization was accomplished by applying 5–10 μl of the freshly-treated thiolated CP solution in a moisture-saturated environment chamber overnight at room temperature. The electrode was then thoroughly cleaned in a copious amount of stirred PBS. To introduce additional anchoring moieties and improve the stability, the CP-coated electrode was subsequently incubated in 2.0 mg/mL MAn in ethanol for 2 h. During incubation, MAn molecules filled in the defects via strong interaction between thiol and gold, forming a mixed monolayer with the CPs. The amino groups on the immobilized MAn molecules serve as anchoring sites for the deposition of PDB film. The surface coverage of the immobilized CPs, estimated electrochemically using $Ru(NH_3)_6Cl_3$ (Steel et al., 1998), was found to be in the range of 6.5–9.8 pmol/cm^2.

2.3. Total RNA extraction and miRNA detection

Total RNA in cultured cells was extracted by using Qiagen's miRNeasy Mini Kit according to the manufacturer's recommended protocol. MicroRNAs in the total RNA were further enriched by using the RNeasy MinElute Cleanup Kit. The yield, quality, and concentration of total RNA were routinely monitored by UV–vis spectrophotometry.

The hybridization of a target miRNA and its electrochemical characterization and EIS detection were performed as follows: First, the biosensor was immersed in the target miRNA solution in a parafilm-sealed small-volume centrifuge tube. The biosensor and the centrifuge tube were placed in a water bath maintained at 10 °C below the melting temperature of the target miRNA. After a 60-min hybridization period, the biosensor was rinsed thoroughly with a blank hybridization buffer at the hybridization temperature. Afterwards, a 30-min incubation of the biosensor in 5 U Nuclease I at 37 °C was performed. PDB deposition was achieved through a period of 60 min incubation in the PDB deposition cocktail. Atomic force microscopic tests confirmed the deposition of PDB on the hybridized biosensor (Fig. S1). Finally, EIS detection was realized in the 0.10 M sodium sulfate containing $Fe(CN)_6^{3-}$/$Fe(CN)_6^{4-}$. For miRNA expression analysis of the members of let-7 family, biosensors coated with respective complementary CPs were used. 5.0-μl aliquots of the total RNA sample solution were dispensed onto the biosensors; hybridization and EIS detection were carried out as described above. To validate the results, the same samples were analyzed by qRT-PCR using a commercial miRNA qRT-PCR kit (Agilent Technologies).

3. Results and discussion

3.1. Label-free miRNA detection mechanism

Fig. 1 illustrates the principal steps of the proposed label-free miRNA biosensor: (a) a monolayer of the CPs is self-assembled onto a gold electrode and MAn is used to fill the defects of the CP monolayer via thiol–gold interaction to improve the quality and stability of the CP monolayer and to provide additional holding power (anchoring sites); (b) the interaction of the CPs with target miRNA strands via base-pairing form duplexes, bringing the miRNA strands onto the biosensor surface; (c) the hybridized biosensor is then incubated in nuclease I in pH 7.4 PBS for 30 min

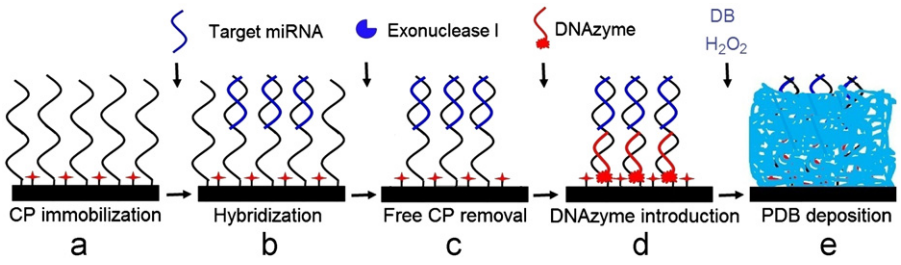

Fig. 1. Schematic illustration of the label-free miRNA biosensor.

at 37 °C; (d) a second hybridization of the oligonucleotide-tailed DNAzyme molecules with the DNAzyme capturing segments at the bottom of the CPs brings the DNAzyme onto the biosensor surface; (e) incubation of the biosensor in the PDB deposition cocktail; and (f) the biosensor is examined by EIS in the $Fe(CN)_6^{3-}$/$(CN)_6^{4-}$ solution after the incubation and compared to that of the control. The engagement of the nuclease clean-up step instead of direct EIS detection is to minimize non-hybridization-related deposition of PDB by removing all free CP strands from the hybridized biosensor as they can also serve as templates for the deposition of PDB. The presence of free CP strands will substantially lift the background signal, and hence the detection limit. In addition, by removing the free CP strands from the biosensor surface, a minimal R_{ct} (background) close to that observed at a bare gold electrode is expected, thus producing a high signal-to-noise (S/N) ratio. During the incubation of the hybridized biosensor in the nuclease I solution, all free CP strands are completely digested by the nuclease (Shimada et al., 2010), leaving only the target miRNA-CP duplexes on the biosensor surface. When the biosensor is further incubated in the PDB deposition cocktail, the hybridized target miRNA-CP duplexes serve as templates, MAn molecules as anchoring sites, and the DNAzyme as initiator for the polymerization of DB and the deposition of PDB. As a result, deposition of PDB occurs exclusively at the hybridized biosensor. The amount of the deposited PDB and its impedance directly correlate to the concentration of the target miRNA in the sample solution.

Arising from the cumulative nature of PDB deposition process, high sensitivity can conveniently be realized if the deposition of PDB is allowed to proceed for an adequately long period of time. The reason of using $Fe(CN)_6^{3-}$/$Fe(CN)_6^{4-}$ instead of other redox probes is two-fold: To maximize the change in charge-transfer resistance (R_{ct}) associated with the hybridization and the deposition of PDB and to have a low threshold of R_{ct}. Because of their moderate electron-transfer rate (Sabatani and Rubinstein, 1987; Finklea et al., 1993), minute changes of the biosensor after hybridization and PDB deposition will be reflected by the changes in its R_{ct}. As we know, electrochemical reversibility and hence R_{ct} of redox probes are influenced by the presence of any insulating material that the redox probes must penetrate to reach the electrode surface. As observed previously (Long et al., 2004, Xie et al., 2004), evidenced by a noticeably increased peak-to-peak potential separation (ΔEp), the redox processes of $Fe(CN)_6^{3-}$/$Fe(CN)_6^{4-}$ became totally irreversible at oligonucleotide coated electrodes even before hybridization, largely due to strong repulsive electrostatic interaction between $Fe(CN)_6^{3-}$/$Fe(CN)_6^{4-}$ and the anionic oligonucleotide-coated electrode (Long et al., 2004). In other words, the oligonucleotide coating greatly impedes the ability of anionic $Fe(CN)_6^{3-}$/$Fe(CN)_6^{4-}$ to reach the electrode surface, thus resulting in a significantly large value of background R_{ct} (Long et al., 2004; Peng and Gao, 2011). This large background R_{ct} could in principle preclude us from developing any ultrasensitive EIS biosensors. Fortunately, the engagement of nuclease I effectively eliminates the unhybridized CP strands, thus producing a minimal R_{ct} at the control while maintaining a high sensitivity to any change brought about by the target miRNA. And the change in R_{ct} is exclusively associated with the target miRNA. On the contrary, if redox probes with ultrafast electron-transfer rates, such as $Ru(NH_3)_6^{3+}$/$Ru(NH_3)_6^{2+}$ and ferrocene derivatives (Sabatani and Rubinstein, 1987), are employed, their R_{ct} will be insensitive to minute changes of the biosensor after hybridizing to low concentrations of the target miRNA because in order to have a noticeable change their electro-transfer rates must be significantly reduced to reach their threshold values. Below the threshold value, EIS is unable to detect any change in R_{ct} as a straight line with a 45° phase angle is persistent due entirely to diffusion (Randles, 1947).

3.2. DNAzyme-catalyzed polymerization of DB

It was reported that peroxidases such as horseradish peroxidase (HRP) effectively catalyze the oxidation of DB and its derivatives in the presence of H_2O_2. Depending on experimental conditions, further oxidation and polymerization of DB are possible (Claiborne and Fridovich, 1979). It was also reported that certain DNAzymes, such as G-quadruplex-hemin DNAzyme, exhibit peroxidase-like activities in the presence of peroxidase substrates and H_2O_2, thus offering new possibilities to engage DNAzymes in biosensor applications (Travascio et al., 2001; Li et al.; 2007; Deng et al., 2008; Yuan et al., 2012). Compared to the bulky and fragile peroxidases, their small size and high chemical stability make them attractive candidates to be used as novel amplification agents in biosensors. In addition, the above studies also provide a good opportunity to the development of EIS biosensors for the detection of miRNAs utilizing the DNAzyme as a signal generator.

To demonstrate this concept, we first evaluated the catalytic activity of the DNAzyme – G-quadruplex hemin – in the oxidation and polymerization of DB. Since the DNAzyme is a peroxidase-like biocatalyst, a wide variety of typical peroxidase substrates, such as DB, 3,3′,5,5′-Tetramethylbenzidine, 4-aminoantipyrine, *o*-phenylenediamine, and dopamine, were initially tested. It was found that all of them can be catalytically oxidized by H_2O_2 in the presence of the DNAzyme. Amongst them, DB showed the best polymerization and target miRNA-guided deposition characteristics. Therefore, DB was chosen in this study. Similar to the HRP-catalyzed oxidation and polymerization of DB (Claiborne and Fridovich, 1979), a light blue color developed immediately after mixing the DNAzyme with 1.0 mM DB and 50 mM H_2O_2. With the advancement of the reaction, the blue color quickly faded away and the solution turned yellow accompanying with the appearance of some brown precipitates (benzidine brown), in line with the HRP-catalyzed oxidation and polymerization of DB (Fig. 2A inset). The blue color at the beginning of the reaction is due to the formation of a charge-transfer complex of between DB and the oxidized DB with two UV–vis absorption peaks at ~390 and 680 nm. These two absorption peaks gradually diminished and a new absorption peak emerged at ~470 nm, in accordance with the appearance of the yellow color (from the final yellow diimine). It was found that the catalytic activity toward the oxidation of DB is strongly pH dependent, attaining its maximal activity at pH 7.0 (Fig. 2B). Moreover, there was a linear correlation between the initial oxidation rate and the concentration of the DNAzyme, suggesting that the DNAzyme catalyzed oxidation of DB is first-order with respect to the concentration of the DNAzyme. This presented an excellent opportunity for the development of the DNAzyme-based biosensor as the linear dependence between the reaction rate and the concentration of the DNAzyme greatly simplifies the relationship between the analytical signal and the target concentration. Detailed kinetic study showed that the catalytic oxidation can be described by the classical Michaelis–Menten model (Michaelis and Menten, 1913). Unlike HRP which can be easily deactivated by a number of factors, such as temperature, acidity of the medium, and concentration of H_2O_2, as a small enzyme mimic the DNAzyme is expected to be very robust. Indeed, the DNAzyme was found to be much more tolerant than HRP in terms of reaction conditions. For example, it was observed that the DNAzyme remains active in a much wider range of H_2O_2 concentration from 50 μM to 200 mM, while HRP was quickly deactivated at >10 mM. The small size, high activity, and high stability make the DNAzyme an attractive reporter (amplifier) in biosensors. As detailed in the subsequent section, an attempt to apply the DNAzyme in the construction of the EIS biosensor for label-free detection of miRNAs was executed.

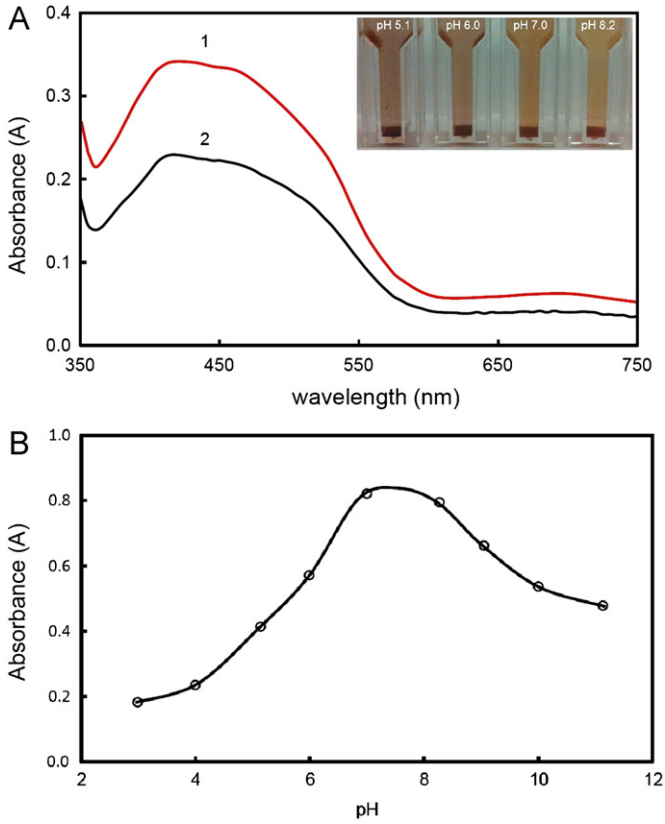

Fig. 2. (A) UV–vis spectra of the oxidation of DB by H_2O_2 in the presence of (1) HRP and (2) the DNAzyme. The reaction mixture contained 1.0 mM DB, 5.0 mM H_2O_2, and 10 ng/mL HRP in pH 5.0. 0.10 M phosphate buffer for (1) and 1.0 mM DB, 12.5 mM H_2O_2, and 0.5 μM DNAzyme in pH 5.0. 0.10 M phosphate buffer for (2); inset: a photograph recording typical solution colors during the DNAzyme-catalyzed oxidation of DB at different pHs; and (B) effect of pH on the DNAzyme-catalyzed oxidation of DB. 1.0 mM DB, 12.5 mM H_2O_2, and 0.5 μM DNAzyme.

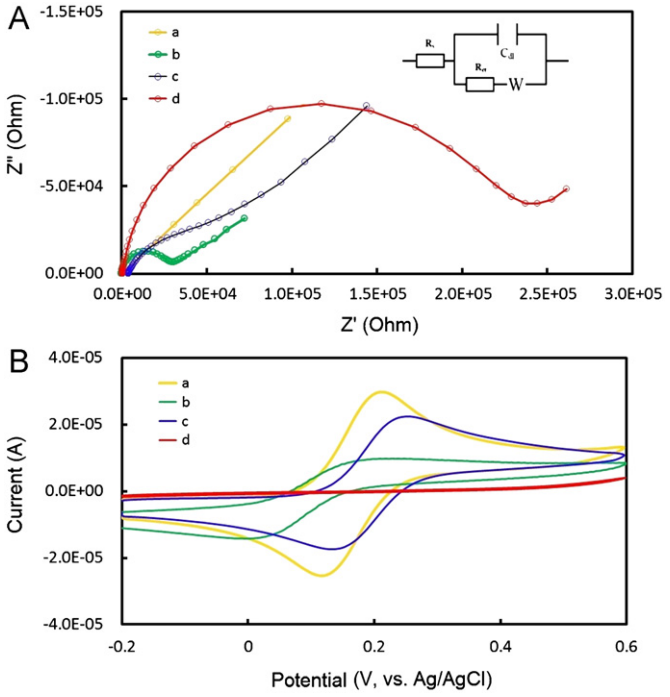

Fig. 3. (A) EIS spectra of $Fe(CN)_6^{3-}/Fe(CN)_6^{4-}$ at (a) the bare gold electrode, (b) the biosensor after hybridization, (c) control, (d) the hybridized biosensor after PDB deposition; and (B) their corresponding cyclic voltammograms. 1.0 pM target miRNA, 60 min hybridization, 30 min incubation in 5 U nuclease I, and 60 min incubation in the PDB deposition cocktail. EIS and voltammetric tests were conducted in 0.10 M Na_2SO_4 containing 2.5 mM $K_3Fe(CN)_6$/2.5 mM $K_4Fe(CN)_6$. For clarity, the EIS spectrum of the control was scaled up 25 times. Inset: Randles equivalent circuit; R_s: solution resistance, C_{dl}: double layer capacitance, R_{ct}: charge transfer resistance, and W: Warburg impedance (diffusion) element.

3.3. Feasibility study

To test the feasibility of utilizing the DNAzyme as an amplifier in ultrasensitive detection of miRNAs, 1.0 pM synthetic let-7c miRNA was tested at the biosensor where the upper segments of the CPs were fully complementary to let-7c and the lower segments fully complementary to the tail of the DNAzyme. In addition, a biosensor coated with CPs fully noncomplementary to Let-7c was used as the control and treated exactly by the same procedures alongside the let-7c biosensor. Upon the second hybridization, the DNAzyme was selectively bound to the lower segments of the CPs and became fixed on the biosensor surface. The incubation in the PDB deposition cocktail resulted in the formation of a thin insulating PDB film on the biosensor surface via the DNAzyme-catalyzed polymerization of DB, akin to that of HRP-catalyzed polymerization of DB (Claiborne and Fridovich, 1979), and the hybridized miRNA-CP duplex-guided deposition of PDB. Additionally, apart from being firmly held by the CP strands, the immobilized MAn molecules provided additional anchoring sites for the deposition of PDB. It has been shown that surface-bonded MAn molecules can form an ordered structure on gold surface. The amino group on the MAn molecules are more reactive than aniline and more easily to be oxidized to the cation radicals, thus participating in the deposition of PDB by serving as the nucleation sites (anchoring sites) for the chain propagation of PDB (Sabatani et al., 1995; Hayes and Shannon, 1996).

Fig. 3 shows typical EIS responses and cyclic voltammograms of the thus treated biosensor and the control. For comparison, the EIS spectrum and cyclic voltammogram of a bare gold electrode were also depicted in Fig. 3. The EIS spectrum of the biosensor was made of a semicircle on high frequency side followed by a straight line with a 45° phase angle on low frequency side (Fig. 3A trace d). The diameter of the semicircle is denoted as the charge transfer resistance, R_{ct}, which is the measure of electron-transfer resistance between the redox probes in solution and the substrate gold electrode through the deposited PDB film. R_{ct} is the key parameter directly correlated with the impeding power of the PDB film, and hence the concentration of the target miRNA. Values of R_{ct} can be conveniently extracted from the EIS spectrum by direct analysis of the spectrum or by fitting the spectrum to the Randles equivalent circuit (Randles 1947) using a complex non-linear regression least-squares program (Zahner Elektrik, Germany) with a data weighting of 2.22. The fitting was considered completed when a modulus impedance error is $\leq 0.25\%$ and phase angle error is $\leq 0.2°$. The straight line, on the other hand, is associated to the diffusion process of the redox probes in solution. And in this case, it is less significant in the detection of miRNAs. As represented by trace a of Fig. 3A, a straight line was observed at the bare gold electrode in the whole frequency range, indicating that R_{ct} of $Fe(CN)_6^{3-/4-}$ at the bare gold electrode is negligibly small and the electrode process is entirely controlled by diffusion in solution. More importantly, the EIS spectrum of the control is close to that obtained at the bare gold electrode and a minimal R_{ct} (background) close to that observed at the bare gold electrode was obtained (trace c of Fig. 3A), due largely to the complete removal of the CP strands by nuclease I. The negligible increment in R_{ct} of the control implies that non-hybridization-related uptake of the target miRNA is insignificant. On the other hand, the substantially larger R_{ct} obtained at the let-7c biosensor

evidently reflected the consequence of the hybridization of the let-7c target and the subsequent DNAzyme-catalyzed deposition of PDB on the biosensor. The hybridization of the target already resulted in a notable increase in R_{ct} (trace b of Fig. 3A) as the presence of the target-CP duplexes on the biosensor efficiently impeded the electron-transfer between the redox probes and the substrate gold electrode. A further ~10-fold increase in R_{ct} was realized after the deposition of PDB (trace d of Fig. 3A). Supportive evidence was found in the corresponding voltammetric responses (Fig. 3B). As another indicator of electron-transfer resistance, ΔE_p, was found in the order of ΔE_p (bare gold) $< \Delta E_p$ (control) $< \Delta E_p$ (hybridized biosensor) $< \Delta E_p$ (hybridized biosensor after PDB deposition), which is in perfect alignment with the magnitudes of R_{ct} observed.

3.4. Analytical characteristics of the biosensor

Under the optimized conditions (See Supporting Information), it was found that R_{ct} of the biosensor is exclusively associated with the concentration of the target miRNA. To establish the quantitative relationship between R_{ct} and miRNA concentration, three synthetic miRNAs, namely miR-720 (17 nucleotides), let-7c (22 nucleotides), and miR-1248 (27 nucleotides), covering from the shortest to the longest miRNAs found in humans, were used as calibration standards to assess the analytical characteristics of the biosensor. For control experiments, a completely noncomplementary 22-nucleotide RNA was used. The 60-min hybridization and 60-min incubation in the PDB deposition cocktail generated a dynamic range from 5.0 fM to 1.0 pM and a detection limit of 2.0 fM at a S/N ratio of 3.0 (Fig. 4A). Tests of 10 individual let-7c biosensors showed that the relative errors associated with the biosensors were generally less than 15% in the concentration range from 20 fM to 1.0 pM. In addition, practically identical sensitivity was observed regardless of the length of the target miRNA. Since the ratio of the DNAzyme to the target miRNA strand is fixed at 1:1, similar sensitivities should be observable for all target miRNAs when hybridizations are performed under similar

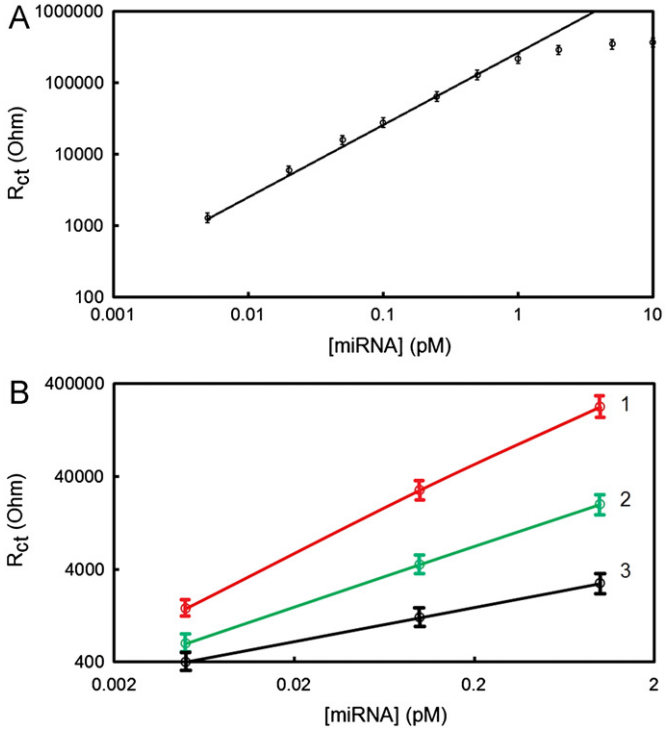

Fig. 4. (A) Calibration curve for miRNA and (B) EIS responses of let-7c biosensors to let-7c, let-7a, and let-7e. Conditions are as for Fig. 3.

Table 1
Analysis of miRNA in total RNA extracted from cultured cells.

Sample	let-7a (10^6 copy/μg RNA)	Let-7b (10^6 copy/μg RNA)	Let-7c (10^6 copy/μg RNA)
HeLa cells	7.6 ± 1.4	25 ± 3.5	6.7 ± 0.95
	(8.2 ± 1.4)*	(23 ± 3.4)	(7.4 ± 0.89)
Lung cancer cells	1.9 ± 0.25	3.0 ± 0.39	2.3 ± 0.38
	(2.2 ± 0.25)	(2.7 ± 0.42)	(2.1 ± 0.29)

* Data in brackets were obtained by qRT-PCR.

stringencies. The sensitivity observed in this work is among the highest of label-free electrochemical biosensors (Table S1) and comparable to that of the RuO_2 nanoparticle-based system (Peng and Gao, 2011), but the elimination of the miRNA tagging step greatly simplifies the assay procedure and enhances the reproducibility.

The specificity of the biosensor was evaluated by analyzing closely associated miRNAs - members of an miRNA family. The let-7c biosensor was therefore employed to analyze let-7c and two interfering miRNAs, namely let-7a (one-base mismatched) and let-7e (two-base mismatched), at 5.0 fM, 100 fM, and 1.0 pM, respectively. As seen in Fig. 4B, persistently lower R_{ct} values were obtained with let-7a and let-7e when they were analyzed by the let-7c biosensor. However, the best selectivity was obtained at 1.0 pM, the upper limit of the calibration curve. The deterioration in selectivity with decreasing target concentration is largely due to the increased contribution from the background R_{ct}. At 1.0 pM, the selectivity factors between let-7c and let-7a, and let-7a and let-7e were found to be 12 and 80, respectively. When three or more bases were mismatched, R_{ct} was found to be indistinguishable from the background. Further confirmation of the selectivity was obtained in an interference study where genomic DNA (from salon sperm) was used. A positive interference of $< 10\%$ was observed when 1.0 pM let-7c was tested in the presence of 6.0 mg/L (~10 μM in base-pairs) the genomic DNA. This level of selectivity between the perfectly complementary and mismatched target is comparable to those reported in most hybridization-based biosensors (Tansil et al., 2005; Sassolas et al., 2008).

In addition to its excellent sensitivity, the label-free approach makes the proposed biosensor particularly attractive for routine miRNA analysis. The freedom from chemical/biological ligation and PCR amplification greatly improves the suitability in direct profiling miRNAs with minimal sample pretreatment. Three representative members of let-7 family were analyzed by their corresponding biosensors, respectively. Aliquots of the total RNA were diluted with the hybridization buffer and directly applied to the biosensors. As references, expression levels of the three miRNAs were simultaneously quantified by a commercial qRT-PCR kit. As listed in Table 1, the results obtained with the biosensors were in good agreement with those obtained by qRT-PCR on the same samples and consistent with published data (Nelson et al., 2004; Allawi et al., 2004). The relative errors associated with the detection of the three miRNAs were less than 20%. With the greatly improved sensitivity, the biosensor significantly reduced the amount of total RNA needed from micrograms to nanograms.

4. Conclusion

In conclusion, attractive analytical characteristics of the DNAzyme-based biosensor for highly sensitive label-free detection of miRNAs were demonstrated in this work. The association of the DNAzyme to the target miRNA led to the unique DNAzyme-catalyzed and the miRNA-CP duplex-guided deposition of insulating PDB film on the biosensor. Being capable of analyzing genomic samples

without PCR amplification and/or ligation and with minimal requirement on sample pretreatment, the proposed biosensor is an attractive candidate for the development of a highly portable device for routine miRNA expression profiling at point-of-care.

Acknowledgment

This work was supported by the A*STAR-ANR Program.

Appendix A. Supporting information

Supplementary data associated with this article can be found in the online version at http://dx.doi.org/10.1016/j.bios.2013.01.028.

References

Allawi, H.T., Dahlberg, J.E., Olson, S., Lund, E., Olson, M., Ma, W.P., Takova, T., Neri, B.P., Lyamichev, V.I., 2004. RNA 10, 1153–1161.
Bartel, D.P., 2004. Cell 116, 281–297.
Chen, C.F., et al., 2005. Nucleic Acids Research 33, e179.
Claiborne, A., Fridovich, I., 1979. Biochemistry 18, 2325–2329.
Deng, M.G., Zhang, D., Zhou, Y.Y., Zhou, X., 2008. Journal of the American Chemical Society 130, 13095–13102.
Engels, B.M., Hutvagner, G., 2006. Oncogene 25, 6163–6169.
Esquela-Kerscher, A., Slack, F.J., 2006. Nature Reviews Cancer 6, 259–269.
Finklea, H.O., Snider, D.A., Fedyk, J., Sabatani, E., Gafni, Y., Rubinstein, I., 1993. Langmuir 9, 3660–3667.
Gao, Z.Q., Yang, Z.C., 2006. Analytical Chemistry 78, 1470–1477.
Gao, Z.Q., Yu, Y.H., 2007. Biosensors and Bioelectronics 22, 933–949.
Li, T., Dong, S.J., Wang, E.K., 2007. Chemical Communications, 4209–4211.
Liang, R.Q., Li, W., Li, Y., Tan, C., Li, J., Jin, Y., Ruan., K.C., 2005. Nucleic Acids Research 33, e17.
Long, Y.T., Li, C.Z., Sutherland, C.T., Kraatz, H.B., Lee, J.S., 2004. Analytical Chemistry 76, 4059–4065.
Lu, J., et al., 2005. Nature 435, 834–838.
Michaelis, L., Menten, M.L., 1913. Biochemistry Zeitung 49, 333–369.
Nelson, P.T., Baldwin, D.A., Scearce, L.M., Oberholtzer, J.C., Tobias, J.W., Mourelatos, Z., 2004. Nature Methods 2, 155–161.
Peng, Y.F., Gao, Z.Q., 2011. Analytical Chemistry 83, 820–827.
Pritchard, C.C., Cheng, H.H., Tewari, M., 2012. Nature Reviews Genetics 13, 358–369.
Qian, H., He, L., 2009. Analytical Chemistry 81, 4536–4542.
Randles, J.E.B., 1947. Discussions of the Faraday Society 1, 11–13.
Raymond, C.K., Roberts, B.S., Garrett-Engele, P., Lim, L.P., Johnson, J.M., 2005. RNA 11, 1737–1744.
Sabatani, E., Rubinstein, I., 1987. Journal of Physical Chemistry 91, 6663–6669.
Sabatani, E., Gafni, Y., Rubinstein, I., 1995. Journal of Physical Chemistry 99, 12305–12311.
Sassolas, A., Leca-Bouvier, B.D., Blum, L.J., 2008. Chemical Reviews 108, 109–139.
Shimada, A., Masui, R., Nakagawa, N., Takahata, Y., Kim, K., Kuramitsu, S., Fukui, K., 2010. Nucleic Acids Research 38, 5692–5705.
Stefani, G., Slack, F.J., 2008. Nature Reviews Molecular Cell Biology 9, 219–230.
Tansil, N.C., Xie, H., Xie., F., 2005. Analytical Chemistry 77, 126–134.
Thomson, J.M., Parker, J., Perou, C.M., Hammond, S.M., 2004. Nature Methods 1, 47–53.
Travascio, P., Witting, P.K., Mauk, A.G., Sen, D., 2001. Journal of the American Chemical Society 123, 1337–1348.
Volinia, S., et al., 2006. Proceedings of the National Academy of Sciences of the United States of America 103, 2257–2261.
Xie, H., Zhang, C.Y., Gao, Z.Q., 2004. Analytical Chemistry 76, 1611–1617.
Yuan, Y.L., Yuan, R., Chai, Y.Q., Zhuo, Y., Ye, X.Y., Gan, X.X., Bai, L.J., 2012. Chemical Communications 48, 4621–4623.